Fast electron transport and induced heating in aluminium foils

J J Santos , A Debayle , Ph Nicolaï , V Tikhonchuk , M Manclossi , D Batani , A Guemnie-Tafo , J Faure , V Malka , J J Honrubia

CELIA, Université Bordeaux 1-CNRS-CEA, Talence, France
LOA, CNRS-ENSTA-Ecole Polytechnique, Palaiseau, France
Dip. Fisica G. Ochialini, Univ. degli Studi di Milano-Bicocca, Milan, Italy
GIFI, Universidad Politécnica, Madrid, Spain

Abstract. Beams of fast electrons have been generated from the ultra-intense laser interaction with Aluminium foil targets. The dynamics of the fast electrons propagation and the level of induced in-depth heating have been investigated using the optical emission from the foils rear side. Important yields of thermal emission, consequence of high target temperatures, were detected for targets thinner than 50 μm. We precisely characterized the targets in-depth temperature profile in order to reproduce the emission yields. At shallow depth, we show the important heating (estimated to $>$ 100 eV till 15 μm depth) has a resistive origin upon the neutralizing return current. For deeper regions, because of the bulk component divergence, the fast electron energy losses and induced heating are due to collisions. Coupling the model to the experimental measurements, we were able to quantify the bulk of the fast electron population, corresponding to 35% of the laser energy and a 500 keV temperature.

1. Introduction

In laser-solid interactions at relativistic intensities ($\geq 10^{18}\,\mathrm{Wcm^{-2}}$), an intense, supra-thermal electron current is created from the plasma at the front side and propagate through the cold interior of the target. It corresponds to currents of about 10^7 A and current density values of about 10^{12}-$10^{13}\,\mathrm{Acm^{-2}}$. These fast electrons transport up to 30-40% of the laser energy focused on target. In this regime, the physics of the electron transport and the energy exchange with the background material is dominated by collective mechanisms associated with the huge fields, spontaneously induced by charge separation and currents. They produce the magnetic focusing of the electron beam, its electric deceleration, the resistive heating of target material and the possibility of the beam filamentation. In addition to these effects one should consider the collisional processes of electrons deceleration and angular diffusion. In this work we developed a simple model for the fast electron transport and induced heating, describing the experimental results from UHI laser interactions with Al foil targets.

2. Model for target heating by the fast electrons

The model assumes a linear growth of the transverse size of the fast electron beam against target depth. It resolves in time the evolution of the background electron temperature considering both

the resistive heating by the return current and the contribution of the fast electron collisions with target electrons (in the Bethe-Bloch approximation). The *ad hoc* injected electron population is defined by 4 parameters, respectively 2 for the geometry of their propagation and 2 for their energy content and spectrum:

- The fast electron radius r_0 and the divergence half-angle θ. At a given depth z into the target, the radius of the incident beam is $r(z) = r_0 + z \tan\theta$.
- The laser energy conversion efficiency into fast electrons η and the temperature of the injected fast electron population T_h. We assume a relativistic Maxwellian energy distribution.

For a characterized fast electron population, the model predicts the yields of the mean background temperature at a given depth into the target , or inversely, the parameters can be adjusted to produce in-depth longitudinal background electron temperature profiles $T_e(z)$ in agreement with measurements or calculations

Figure 1 synthesizes the main optical emission results from an experiment performed at LOA . The intense laser pulses (0.7 J, 40 fs, $6\,10^{19}$ Wcm^{-2} at 815 nm) were focalized into Al foil targets: panel a) shows the 525 ± 45 nm emission radius connected to the fast electron flux (green symbols) against target overdense thickness (estimated from hydrodynamic simulations upon the effect of the laser ASE-prepulse). According to the data, the model's geometry parameters should be fixed within the intervals $r_0 \sim$ 3-10 μm and $\theta \sim$ 30-40°. η and T_h are taken as free parameters. Panel b) shows the emission energy against foil thickness for two spectral regions, 405 ± 5 nm (corresponding to the laser second harmonic $2\omega_0$, open purple symbols) and 546 ± 5 nm, not connected to any laser harmonic and called *visible* light (full green symbols). For the thinner targets, the *visible* light is practically only of thermal origin, the trace of the moderately relativistic bulk of the accelerated electrons, whereas the $2\omega_0$ light has both thermal and Coherent Transition Radiation (CTR) contributions. The CTR, produced by a micro-bunched and collimated relativistic tail of the fast electrons energy distribution, domains the emission for the thicker targets on both spectral regions [1].

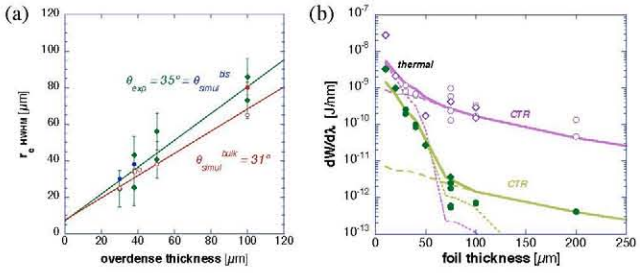

Figure 1. a) Radius of the fast electrons jets against the foils overdense thickness (as computed by hydrodynamic simulations): green diamonds are the experimental 525 ± 45 nm bright spots, open red circles are the model estimates for the background electron temperature. Full red circle and full blue circles correspond respectively to model corrections accounting for thermal energy expansion and to fast electron refluxing. b) Integrated energy against Al foil thickness for the $2\omega_0$ and *visible* signals (respectivelly purple and green symbols): they are fitted (solid curves) by the added contribution of the CTR (dashed) and thermal (dotted) radiation models.

The fast electron current $\overrightarrow{j_h}$ produces an electrostatic field $\overrightarrow{E}$ that slows down the fast electrons. This field produces a return current of the target free electrons, according to the Ohm's law $\overrightarrow{j_e} = \sigma \overrightarrow{E}$. We assume a complete current neutralisation ($\overrightarrow{j_e} = -\overrightarrow{j_h}$) and use the metal return electron energy equation to quantify the deposited energy per unit volume and time: $1.5 C_V \frac{dT_e}{dt} = \overrightarrow{E} \cdot \overrightarrow{j_e} = \frac{j_h^2}{\sigma}$. Here, σ and C_V are respectively the electrical conductivity and the heat capacity of the target material.

The Al electrical conductivity is calculated from a two-temperature model by B. Chimier *et al.*

For electron temperatures greater than the Fermi temperature $T_e > T_F$, the conductivity

corresponds to the Spitzer theory $\sigma \propto T_e^{3/2}$, and for $T_e < T_F$, it sums the contribution of both the electron-ion $\nu_{ei} \propto T_i$ and electron-electron $\nu_{ee} \propto T_e^2$ collision frequencies. Due to the rapidity of the heating process < 0.5 ps, which is shorter than the electron-ion energy exchange time ~ 2 ps, we assume the ions to be cold: $T_e \gg T_i \sim 0.03$ eV. The same reasoning allows us to neglect the thermal conduction and expansion of the target during the energy deposition.

The best agreement between model and experiment was found for the set of parameters $r_0 = 7.5\,\mu$m and $\theta = 35°$ (from experimental data, Fig. 1-a, also accounting for the fast electron refluxing on the thinner targets), $\eta = 35\%$ (reasonable for the $6\,10^{19}$ Wcm^{-2} laser intensity and known scale laws) and $T_h = 500$ keV (see Fig. 3 further below). For a solid (2.7 g/cm^3) and initially cold (0.03 eV) Al foil, we plot in Fig. 2-a the final electron temperature against the target depth due to the resistive heating mechanism, labeled as $T_e^{\rm ohm}$. It decreases very rapidly with the target depth as it depends on the square of the incident current density $j_h = I_h/(\pi r(z)^2)$. The total current I_h decreases slightly with the depth due to velocity dispersion of the electron bunch. The current density j_h is mostly affected by the transverse broadening due to beam divergence, which predicts a $T_e^{\rm ohm}(z) \propto r(z)^{-4}$ behavior.

Because of the incident beam divergence, after a certain depth, the effects of individual inelastic collisions of the fast electrons with target atoms should become comparable with the resistive losses. The background heating due to collisions is calculated according to the local heat capacity and the Bethe-Bloch stopping power, integrating over the fast electron distribution for each target depth. For the incident energy (~ 0.1-10 MeV) and crossed thickness ($< 200\,\mu$m) ranges, the background heating due to collisions against depth is essentially determined by the fast electrons radial spreading: The result $T_e^{\rm coll}$, blue curve in Fig. 2-a, shows the expected $T_e^{\rm coll} \propto j_h \propto r(z)^{-2}$ behavior.

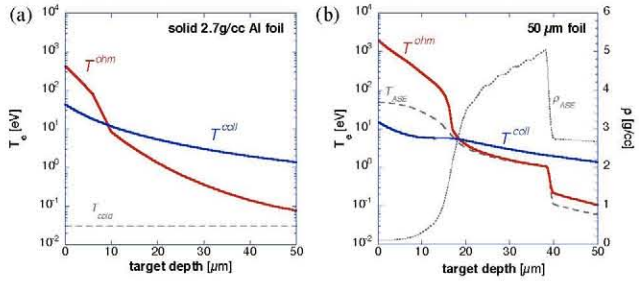

Figure 2. Heating of unperturbed solid (a) and ASE-perturbed (b) Al foils with collisions (blue) and resistive (red curves) contributions. Density and initial temperature profiles are shown in grey.

In order to reproduce our experimental conditions when solving the heating equations, we account for the ASE-induced hydrodynamic effects and input for each Al foil initial density and temperature profiles according to 1D hydrocode simulations (e.g. grey profiles in Fig. 2-b). For both unperturbed solid (Fig. 2-a) and ASE-expanded (Fig. 2-b) Al foil targets, the fast electron energy deposition is dominated by the resistive mechanism till $\approx$ 10-15 μm depth and then by collisions. Nevertheless, across the density gradient at shallow depth, the resistive heating by return currents is significantly enhanced in ASE-expanded foils, where matter is only slightly overdense, its conductivity being quite lower

The model has been successfully validated for targets thicker than 30 μm in comparison to more complete hybrid (particle-fluid) simulations: A good T_e profile agreement is found between model and simulation results [1]. For foils $< 30\,\mu$m, the non-linear growth of the heated region radius, due mostly to the electron magnetic guiding at shallow depth, results in a mismatch between the model and the simulation profiles.

3. Relaxation of an instantaneously heated plasma

We consider an instantaneously heated plasma as the origin of the measured thermal emission. The temperature $T(z)$ is much higher on the front side than on the rear side. The density profiles, given by the hydrodynamic calculations, are not uniform either. After energy deposition

by the fast electrons at time $t = t_h$, the heated plasma volume releases its energy, within a ns time scale, both radially into the surrounding cold material, and axially into vacuum. The longitudinal expansion rules the energy releasing and cooling of the plasma We rely on a 1D longitudinal description for the plasma expansion and thermal emission.

The targets are optically dense for the studied wavelengths (optical range), but one can not suppose the detected radiation is only due to the targets rear side heated surface. Within the 5 ns recording time, due to thermal diffusion and plasma expansion, the electromagnetic emission from the rear surface is sensitive to its interior temperature profile, ranging from a few keV to eV (cf. Fig. 2), and to the target thickness. We show the initial temperature and density profiles are dramatically changed after a few tens or a few hundred of ps by radiation and thermal conduction and under the shock launched from the laser side hot zone

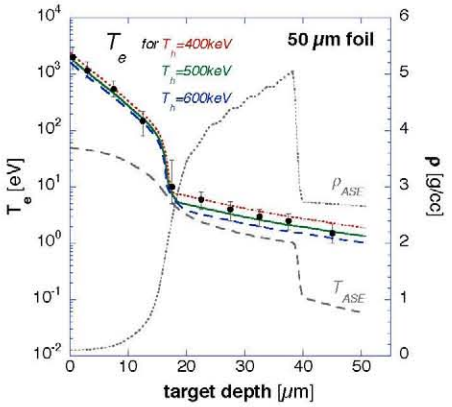

Figure 3. In-depth heating of an ASE-perturbed 50 μm Al foil. Black symbols give the temperature profile at $t = t_h$ reproducing the *visible* emission data. They are fitted by model calculations (colored curves).

Using again hydrodynamic simulations with radiative transport, we could reconstitute the mean T_e longitudinal profile created by the fast electron beam: We injected initial profiles for the density (previous hydrodynamic simulations for the ASE laser pre-pulse effect) and adjusted the in-depth temperature profiles $T(z)$ till we reproduced the best possible the experimental emission yields against target thickness (Fig. 1-b). Black symbols on Fig. 3 show the best temperature profile for the 50 μm foil target. The best agreement with the heating model (colored curves) is found for $T_h \approx 500$ keV, corresponding to $\approx 5\,10^{12}$ accelerated electrons. Except for the 10 μm initial foil thickness, where the integrated emission can not be reproduced by a factor of 4, one can use the same $T(z)$ profile for all Al foils. For foils $> 50\,\mu$m, we have to also consider the CTR contribution to the optical emission

4. Conclusions

We developed a simple model for the fast electron transport in metal layers and induced heating, including resistive effects associated to the self-generated fields and collisions. It accounts for a detailed description of the hydrodynamic effects from the laser ASE-prepulse and of the transient non-equilibrium electric behavior. We also studied the plasma expansion and thermal emission which follows the energy deposition by the fast electrons.

The model first proved to describe the macroscopic characteristics (main divergence, spatial and temporal resolution of the energy deposition) of the bulk of the fast electron population generated in an experiment performed at LOA with a 40 fs duration, $6\,10^{19}$ Wcm^{-2} at 815 nm wavelength It can be easily dimensioned for other laser systems and interaction conditions, as already done for an experiment performed at LULI with a 500 fs duration, 2-3 10^{19} Wcm^{-2} at 1.06 μm wavelength

References

Santos J J *et al.* 2007 *Phys. Plasmas* **14** 103107
Malka G *et al.* 2007 submitted to *Phys. Rev.* E
Chimier B *et al.* 2007 *Phys. Rev.* B **75** 195124